Multi-Period Power System Risk Minimization Under Wildfire Disruptions

Hanbin Yang , Noah Rhodes , Student Member, IEEE, Haoxiang Yang , Member, IEEE, Line Roald , *Member, IEEE*, and Lewis Ntaimo

Abstract—Natural wildfire becomes increasingly frequent as climate change evolves, posing a growing threat to power systems, while grid failures simultaneously fuel the most destructive wildfires. Preemptive de-energization of grid equipment is effective in mitigating grid-induced wildfires but may cause significant power outages during natural wildfires. This paper proposes a novel twostage stochastic program for planning preemptive de-energization and solves it via an enhanced Lagrangian cut decomposition algorithm. We model wildfire events as stochastic disruptions with random magnitude and timing. The stochastic program maximizes the electricity delivered while proactively de-energizing components over multiple time periods to reduce wildfire risks. We use a cellular automaton process to sample grid failure and wildfire scenarios driven by realistic risk and environmental factors. We test our method on an augmented version of the RTS-GLMC test case in Southern California and compare it with four benchmark cases, including deterministic, wait-and-see, and robust optimization formulations as well as a comparison with prior wildfire risk optimization. Our method reduces wildfire damage costs and loadshedding losses, and our nominal plan is robust against uncertainty perturbation.

Index Terms—Decomposition algorithm, de-energization, Lagrangian cut, optimal power flow, stochastic mixed-integer programming, wildfire risk.

NOMENCLATURE

Indices and Index Sets

 \mathcal{B} set of buses.

 \mathcal{G} set of generators.

set of transmission lines.

Manuscript received 7 April 2023; revised 25 July 2023 and 7 November 2023; accepted 19 November 2023. Date of publication 25 January 2024; date of current version 21 August 2024. The work of Hanbin Yang and Haoxiang Yang was supported by the National Natural Science Foundation of China under Grant 72201232 and 72231008. The work of Noah Rhodes and Line Roald was supported in part by the U.S. National Science Foundation ASCENT Program under Grant 2132904 and in part by the Department of Energy, Office of Science, Office of Advanced Scientific Computing Research, Applied Mathematics Program under Grant DE-AC02-06CH11347. Paper no. TPWRS-00501-2023. (Corresponding author: Haoxiang Yang.)

Hanbin Yang and Haoxiang Yang are with the School of Data Science, Chinese University of Hong Kong - Shenzhen, Shenzhen 518172, China (e-mail: hanbinyang@link.cuhk.edu.cn; yanghaoxiang@cuhk.edu.cn).

Noah Rhodes and Line Roald are with the Electrical and Computer Engineering, University of Wisconsin-Madison, Madison, WI 53706 USA (e-mail: nrhodes@wisc.edu; roald@wisc.edu).

Lewis Ntaimo is with the Industrial and Systems Engineering, Texas A&M University, College Station, TX 77843 USA (e-mail: ntaimo@tamu.edu).

Color versions of one or more figures in this article are available at https://doi.org/10.1109/TPWRS.2023.3339147.

Digital Object Identifier 10.1109/TPWRS.2023.3339147

 \mathcal{D} set of load demand.

 \mathcal{C} set of load components, $C = B \cup G \cup L$.

 \mathcal{T} set of time periods, $\mathcal{T} = \{1, 2, \dots, T\}$.

index set of wildfire scenarios.

set of affected components by component c's ignition

under scenario $\omega \in \Omega$.

Parameters

load $d \in \mathcal{D}$ at time period $t \in \mathcal{T}$. D_{dt}

the priority level of load $d \in \mathcal{D}$. w_d

repair cost for component $c \in \mathcal{C}$.

maximum and minimum generation limits of $g \in \mathcal{G}$.

the thermal power flow limit of the line $(i, j) \in \mathcal{L}$.

the susceptance of the line $(i, j) \in \mathcal{L}$.

 b_{ij} $\underline{\theta}, \overline{\theta}$ the big-M values for voltage angle difference.

disruption time for scenario $\omega \in \Omega$.

1 if component $c \in \mathcal{C}$ faults under scenario $\omega \in \Omega$, 0 otherwise.

1 if component $c \in \mathcal{C}$ is shut off by exogenous fire

under scenario $\omega \in \Omega$, 0 otherwise.

Decision Variables

phase angle of the bus $i \in \mathcal{B}$ at time $t \in \mathcal{T}$.

active power flow on the line $(i, j) \in \mathcal{L}$ at time $t \in \mathcal{T}$.

active power generation at generator $g \in \mathcal{G}$ at time

 $t \in \mathcal{T}$.

percentage of demand satisfied at the load $d \in \mathcal{D}$ at x_{dt}

time $t \in \mathcal{T}$.

1 if component $c \in \mathcal{C}$ is functional at time $t \in \mathcal{T}$, 0 z_{ct}

1 if component $c \in \mathcal{C}$ is functional at time $t \in \mathcal{T}$

under scenarios $\omega \in \Omega$, 0 otherwise.

1 if a fire damage is incurred at component $c \in \mathcal{C}$ at η_{ct}^{ω}

time $t \in \mathcal{T}$ under scenarios $\omega \in \Omega$, 0 otherwise.

I. INTRODUCTION

ILDFIRE-RELATED disasters have become more frequent and severe in recent years across the United States [1], [2]. A major aspect of the wildfire research focuses on wildfire mitigation plans in power systems [3]. There is a mutual impact between wildfire ignition and power system operations: on the one hand, many catastrophic fires with significant loss of life and property were sparked by power infrastructures; for example, the Camp Fire in 2018, sparked by a transmission line, caused 84 lives deaths and an estimated \$9.3 billion in residential

0885-8950 © 2024 IEEE. Personal use is permitted, but republication/redistribution requires IEEE permission. See https://www.ieee.org/publications/rights/index.html for more information.

property damage alone [4]; on the other hand, regardless of the source, wildfires lead to damages in power system components, which change the topology and resource availability within a power system [5].

Utility companies have considered approaches in different time scales to reduce the risk of wildfire ignitions [3]. Long-term approaches can last for years, such as equipment inspection, hardening, and vegetation management [6], may require enormous costs and qualified personnel and should be complemented with day-to-day operations such as public safety power shut-offs (PSPS) [7] to eliminate risk. In this paper, we focus on optimizing the operational de-energization decisions over a short time horizon similar to the setup in [8].

When optimizing the de-energization decisions, many previous works mainly focus on wildfire risks caused by power system components but overlook the simultaneous natural/man-made wildfires' damage on power systems [1], [9], [10]. In addition, previous literature and industry practices take a deterministic approach because it is computationally challenging to solve optimization under uncertainty models with binary variables for de-energization, such as a wildfire hazard prevention system based on data mining techniques [11], risk-based optimization models for de-energization [8], [12], a data-driven wildfire decision-making framework for power system resilience [13], and industry practices using thresholds to indicate when to shut off [3], [14]. However, incorporating wildfire spread dynamics can significantly improve the performance of de-energization. Recently, more models have started to incorporate stochastic aspects of wildfire risks, such as a dynamic programming model to optimize a PSPS [15], a two-stage robust optimization model for capacity expansion considering PSPS [16], a two-stage stochastic integer program solved by progressive hedging [17], and rolling horizon optimization models for joint de-energization and restoration [18], [19]. That said, most of the literature still carries a relatively simple decision structure and cannot fully capture the temporal dynamics of the wildfire; for example, a commonly used uncertainty set in robust optimization, such as a budgeted uncertainty set [20], can only capture the number of damaged components, but is not able to accurately characterize the temporal effect of wildfire progress within a multi-period horizon. Therefore, it requires new studies to examine the interaction between power system operations with high-fidelity and dynamic wildfire progress [21].

To holistically analyze the two-way impact between the wild-fire ignitions and the power system operations, we classify wildfires into two categories, *exogenous* and *endogenous* fires: exogenous fires are external to the power system, while power system faults trigger endogenous fires. Extreme weather conditions such as drought [22] can lead to exogenous wildfires, which may cause damages in power system components; e.g., dysfunctional shunts [23], utility-scale converters [24], and line conductors [25]. Endogenous fires are ignited when downed transmission lines come into contact with surrounding vegetation and can damage nearby power system components [8]. A framework to assess endogenous wildfire risk is proposed in [26], and simulation models based on such risk measures can provide early warnings [27]. In this paper, we explicitly

model both exogenous and endogenous wildfires' impact via binary parameters indicating whether either wildfire damages each power system component in every period.

Optimizing a sequential decision process that models shut-off and power flow decisions requires solving a multistage stochastic program. This can be challenging because the computational complexity increases exponentially with the planning horizon length [28], and there may be integer variables involved [8]. We develop a two-stage stochastic mixed-integer programming (SMIP) model that captures the interaction between power system de-energization and both exogenous and endogenous wildfires over multiple periods. We minimize our wildfire risk measure, the expected total cost that incorporates the wildfire damage cost and the load-shedding cost. In addition, our two-stage SMIP model incorporates the spatial and temporal uncertainty of wildfires and represents real-world situations with disruption scenarios, which can handle complex and dynamic situations better and produce more resilient operations than deterministic models. We use a cellular automaton process to simulate wildfire spread and generate scenarios that describe the magnitude and timing of wildfire disruptions. Since wildfire occurs infrequently, we assume at most one wildfire occurrence during the planning horizon to reduce the multi-period problem into two stages [29]. This two-stage scenario-based setting fits the low-probability high-impact property of wildfire ignition and can capture the dynamics of wildfire progress with a high fidelity. We design a proactive scheme that executes an effective de-energization plan before the wildfire and optimizes power flow operations of the remaining available components afterward.

We propose a decomposition algorithm for the two-stage SMIP with non-convex and non-smooth value functions. Our algorithm uses linear cutting planes, named *Lagrangian cuts*, to approximate the value functions [30]. The vanilla version of Lagrangian cuts is tight theoretically but can be inefficient computationally. To overcome this limitation, we introduce an enhanced version of the Lagrangian cut, named *square-minimization cut*, which improves the quality of the approximations and speeds up the algorithm. Our method shows high computational accuracy and reliability. The two-stage SMIP model supports the decision-making process under uncertainty, reduces the likelihood of a disaster, and maintains as much load delivery as possible after a disruption.

The contributions of our paper are fourfold:

- We propose a cellular automaton model that simulates the onset and spread of exogenous and endogenous wildfires based on environmental data. This enables us to assess wildfire risk through scenarios used in the SMIP model.
- 2) We formulate a two-stage SMIP model that manages wildfire risk in power system operations. Unlike the existing literature, our model captures the random nature of wildfire ignitions using disruption scenarios with random onset times to keep the model size manageable.
- We develop a cutting plane algorithm that solves the SMIP model with a finite convergence guarantee. We improve its computational performance significantly with a new square-minimization cut.

4) We show our two-stage SMIP model yields significantly more resilient solutions than its deterministic counterparts and more economical solutions than the robust optimization model. We also analyze the solution under different parametric settings to gain operational insights.

The rest of the paper is organized as follows: Section II presents the wildfire simulation model and the SMIP formulation; Section III derives the cutting plane algorithm and its computational enhancement; Section IV covers benchmark cases and numerical analyses; and Section V concludes the paper with a brief discussion of future work.

II. TWO-STAGE SMIP MODEL

We consider multi-period dispatch and de-energization operations under wildfire disruption over a short-term time horizon (24 hours). The power network is represented by a graph $(\mathcal{B}, \mathcal{L})$, where \mathcal{B} is the set of buses and \mathcal{L} is the set of lines. We use $\mathcal{D}_i, \mathcal{G}_i$, and \mathcal{L}_i to represent the subset of loads, generators, and transmission lines connected to bus i, respectively. For each period $t \in \mathcal{T}$, we formulate DC power flow constraints to decide the active power generation P_{gt}^G of generator $g \in \mathcal{G}$, the power flow P_{ijt}^L on transmission line $(i,j) \in \mathcal{L}$ from bus i to bus j, and the phase angle θ_{it} of bus $i \in \mathcal{B}$.

In our model, we define wildfire risk as the combined cost of load-shedding and wildfire damage under uncertain wildfire disruption over the specified time horizon. In model (1), a de-energized generator will have zero generation capacity, and a de-energized line will be considered open. If a bus is shut off, all generators and lines connected to it will also be de-energized. Our model uses binary decision variables z_{ct} to represent whether a component $c \in \mathcal{C}$ is de-energized at time period t. We assume that a de-energized component will remain off until the end of the time horizon due to safety considerations [8]. Model (1) obtains a first-stage plan, i.e., a nominal plan, that should be implemented until a disruption occurs or the time horizon ends, whichever occurs first. If a fire disruption is observed at period τ^{ω} , given the current shut-off state $z_{\tau^{\omega}-1}$, the model enters the second stage and incurs the second-stage value function f^{ω} , where we assume that the components at revealed ignition locations will be shut off.

A. Wildfire Scenario Modeling

On top of the constructed electric power network, we model wildfire uncertainty as a stochastic disruption with random occurrence timing, location, and spread. We consider a short-term operation and thus assume at most one disruption will occur over the time horizon. We form a portfolio of disruption scenarios indexed by $\omega \in \Omega$, within which we model i) endogenous fires, which are caused by faults of operating electric components, and ii) exogenous fires, which are caused by random natural wildfire ignitions.

We consider the smallest rectangular area that can cover the entire power network and divide it into a two-dimensional grid of a specified resolution, in which the set of cells is denoted by \mathcal{K} . We then construct a mapping between the grid cells and the buses and transmission lines based on their geographic locations.

We let $k_i \in \mathcal{K}$ denote the cell where the bus i is located. A transmission line, l = (i, j), can span multiple cells, which is denoted by \mathcal{K}_{ij} . Furthermore, a cell $k \in \mathcal{K}$ can contain multiple transmission lines, and we denote the set of transmission lines passing cell k by \mathcal{L}^k . Finally, we let $\mathcal{K}_{\mathcal{B}}$ and $\mathcal{K}_{\mathcal{L}}$ be the collection of cells containing at least a bus and at least a transmission line, respectively.

We employ the cellular automaton method, with propagation rules listed in [31], to simulate the spread of exogenous wildfires. Overall, this setup leads to a wildfire disruption in approximately 95% of scenarios. Each cell is characterized by four states which evolve in discrete time. The four states are as follows: (i) cell has no forest fuel; (ii) cell has forest fuel that has not ignited; (iii) cell has ignited forest fuel; (iv) cell has fully burning forest fuel. Endogenous disruptions are caused by power system component failures. The status of each component is normal, at fault, or ignited. We define the onset time of a wildfire disruption τ^{ω} as the earlier time between an exogenous wildfire occurrence and any electric component's fault.

- a) Exogenous wildfires: We assume that there are no exogenous wildfires in the grid at the start of the time horizon. For each cell $k \in \mathcal{K}$ in period $t \in \mathcal{T}$, it receives information from the environment to update its state and interacts with surrounding cells based on a set of defined rules:
 - 1) if its state in period t-1 is the unburned fuel state (ii), it has a probability p_{tk} , influenced by environmental factors, to be ignited and its state will transfer from (ii) to the ignited fuel state (iii);
 - 2) if its state in period t-1 is (iii), then the state will transfer to the fully burning state (iv);
 - 3) if it is a fully burning cell, the state will stay at (iv) and can spread flames to its 8 adjacent cells indexed by k', igniting them with probabilities $q_{tk'}$ if they are in status (ii), where parameters $q_{tk'}$ are subject to environmental factors like vegetation, ground elevation, and wind.

We record the exogenous wildfire damage after the end of time horizon \mathcal{T} , letting $v_c^{\omega} = 1$ if a wildfire (state (iii) or (iv)) ever occurs on k_i if c is bus i or any generator connected to bus i, or on any cell in \mathcal{K}_{ij} , if c is transmission line (i, j).

- b) Endogenous wildfires: We simulate endogenous wildfires using a two-step procedure:
 - 1) First, we simulate electrical component faults. To initialize the fault simulation process, we assume there is no fault component in the power system at the start of the time horizon, similar to the exogenous wildfire simulation. For every period $t \in \mathcal{T}$, a fault may occur at a component $c \in \mathcal{C}$ following a Bernoulli distribution with probability p_{tc} . Once a component faults, we record the state by letting $u_c^\omega = 1$.
 - 2) Our second step runs an independent cellular automaton process for each fault component c from the fault period to the end of the time horizon, initialized with the cell(s) that contains the component in state (iii). After the cell evolves to state (iv) in the next period, it will spread the simulated wildfire to the adjacent cell k' with a probability $q_{t,k'}$ at time period t and further propagate. The components damaged by this spread in the time horizon form a set I_c^c .

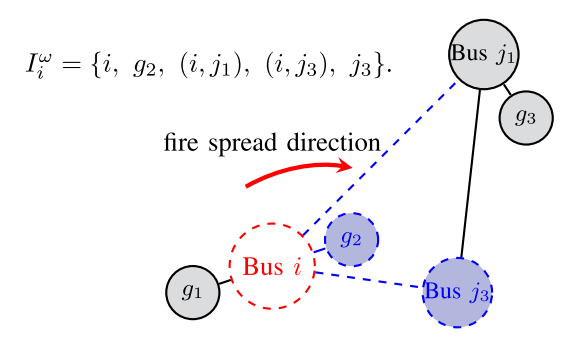


Fig. 1. Random set I_i^{ω} illustration. A fault occurs at bus i (energized), which causes an endogenous wildfire to spread and affect two transmission lines (i,j_1) and (i,j_2) , bus j_3 , and generator g_2 , which are marked by blue dashed lines.

Fig. 1 provides an illustration of a set of components affected by an endogenous fire: a fault occurs at an energized bus i, igniting an endogenous wildfire and impacting two transmission lines, a bus, and a generator (marked by dashed lines). Notice that we assume a fault directly leads to a wildfire because we aim to simulate how an endogenous fire would spread if the component c were not de-energized. In addition, we build independent simulation processes, each starting with only the cell(s) containing the fault component c, in order to clearly trace the spread of a wildfire to its origin and eliminate the interference of endogenous wildfires started elsewhere.

In summary, for a specific scenario $\omega \in \Omega$, we use a cellular automaton procedure to generate the wildfire disruption uncertainty $\xi^\omega = \{\tau^\omega, v^\omega_\cdot, u^\omega_\cdot, I^\omega_\cdot\}$, which includes the disruption time τ^ω , the binary parameters v^ω_c indicating the exogenous fire locations, the binary parameters u^ω_c indicating the fault locations, and the set I^ω_c characterizing components damaged by the potential endogenous fire at component c. We detail the parameter setup:

Mapping onto Grid: We convert the location of each bus $i \in \mathcal{B}$ from latitude and longitude [32] to Universal Transverse Mercator(UTM) coordinates [33]. The smallest rectangle that contains the entire power network has a length of 180,000 and a width of 138,000 UTM unit. We divide such a rectangular area into square cells with an edge length of 1,000 UTM units. Such edge length ensures a high resolution of our simulation model and is in the same order of magnitude as the average distance that a wildfire can spread within a time period.

Probability of Exogenous Wildfire Ignition p_{tk} : We assume that only wildfires that occur in cells with at least one power system component will threaten the electric power system. As stated in Section II-A, we model the ignition of exogenous wildfires at time t by a probability p_{tk} , which describes the likelihood of a cell $k \in \mathcal{K}$ transitioning from the state (ii), un-burned fuel, to state (iii), ignited the fuel. To estimate p_{tk} , we use the Wildland Fire Potential Index (WFPI) [34] as a measure of the relative probability of ignition. The probability of an exogenous wildfire occurring in cell k in which the set of all transmission lines passing through cell k is \mathcal{L}^k is

$$p_{tk} = \frac{\sum_{l \in \mathcal{L}^k} \mathtt{WFPI}_l}{\sum_{l' \in \mathcal{L}} \mathtt{WFPI}_{l'}}.$$

Probability of Wildfire Spread $q_{tk'}$: Suppose there is a fully burning cell. Each of the adjacent cells $k' \in \mathcal{K}$ will be ignited with probability $q_{tk'}$. This probability $q_{tk'}$ depends on: 1) a reference probability that cell k' will be burning under no wind and flat terrain, $q_{0k'}$; 2) the vegetation type, $q_{k'}^{\text{veg}}$, and vegetation density, $q_{k'}^{\text{den}}$; 3) geographical information, $q_{k'}^{s}$; and (iv) wind speed and direction, $q_{k'}^{w}$, as follows:

$$q_{tk'} = q_{0k'} \left(1 + q_{k'}^{\text{veg}} \right) \left(1 + q_{k'}^{\text{den}} \right) q_{k'}^s q_{tk'}^w.$$

We refer to Ref. [31] and [35] for detailed parameter values.

Probability of Fault p_{tc} : Transmission lines are more prone to failures than other electrical components due to environmental factors such as lightning and wind [36]. Therefore, in our implementation, we focus on the fault at transmission lines and set $p_{tc} = 0, \forall c \in \mathcal{B} \cup \mathcal{G}$. This setup can be easily extended if we want to consider the risk of fault at buses and generators. In any time period, we assume a constant fault probability for each line $l \in \mathcal{L}$ as $p_{tl} = 1 - e^{-\bar{\lambda}}$, where $\bar{\lambda}$ is the estimated hourly failure rate in the Poisson regression model of [36].

B. Two-Stage SMIP Model

When a fault occurs at an energized component, the associated endogenous wildfire may incur high damage costs. To reduce the endogenous risk of igniting a wildfire, the power system operator can de-energize, i.e., shut off, power equipment. However, suppose multiple components are de-energized to prevent endogenous fires. In that case, the power supply capacity may be greatly reduced, resulting in the inability to meet crucial load demand and causing serious secondary disasters. To improve the reliability of the power system and mitigate wildfire damage, operators should de-energize some potentially dangerous electrical equipment under high-risk conditions to ensure enough power supply while significantly reducing risk.

To achieve a balanced risk trade-off between endogenous fire and load-shedding, we build a two-stage SMIP model (1) which optimizes shut-off decisions under wildfire disruption uncertainty over the given time horizon. In model (1), a de-energized generator will have zero generation capacity, and a de-energized line will be considered open. If a bus is shut off, all generators and lines connected to it will also be de-energized. Our model uses binary decision variables z_{ct} to represent whether a component $c \in \mathcal{C}$ is de-energized at time period t. We assume that a de-energized component will remain off until the end of the time horizon due to safety considerations [8]. Model (1) obtains a first-stage plan, i.e., a nominal plan, that should be implemented until a disruption occurs or the time horizon ends, whichever occurs first. If a fire disruption is observed at period τ^{ω} , given the current shut-off state $z_{\tau\omega-1}$, the model enters the second stage and incurs the second-stage value function f^{ω} , where we assume that the components at revealed ignition locations will be shut off.

$$Z^* = \min \sum_{\omega \in \Omega} p^{\omega} \left[\sum_{t=1}^{\tau^{\omega} - 1} \sum_{d \in \mathcal{D}} w_d (1 - x_{dt}) + f^{\omega}(z_{\tau^{\omega} - 1}, \xi^{\omega}) \right]$$
s.t. $\forall t \in \mathcal{T}$:

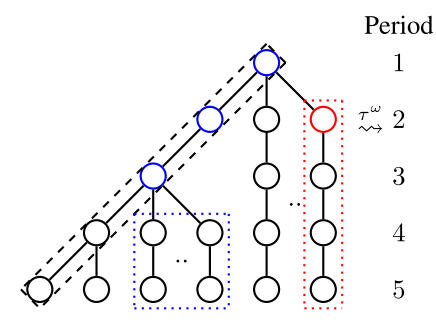


Fig. 2. Scenario-tree illustration of the wildfire disruption problem with T=5 and $\tau^\omega=2$. The branch in the red box represents the disruptive scenarios where the disruption occurs in period 2. The branches in the blue boxes represent the scenarios sharing the same historical information (the nodes in blue).

$$\begin{split} P_{ijt}^L & \leq -b_{ij} \left(\theta_{it} - \theta_{jt} + \bar{\theta} (1 - z_{ijt}) \right) & \forall (i,j) \in \mathcal{L} \quad \text{(1a)} \\ P_{ijt}^L & \geq -b_{ij} \left(\theta_{it} - \theta_{jt} + \underline{\theta} (1 - z_{ijt}) \right) & \forall (i,j) \in \mathcal{L} \quad \text{(1b)} \\ -W_{ij} z_{ijt} & \leq P_{ijt}^L \leq W_{ij} z_{ijt} & \forall (i,j) \in \mathcal{L} \quad \text{(1c)} \\ \sum_{g \in \mathcal{G}_i} P_{gt}^G + \sum_{l \in \mathcal{L}_i} P_{lt}^L & = \sum_{d \in \mathcal{D}_i} D_{dt} x_{dt} & \forall i \in \mathcal{B} \quad \text{(1d)} \\ P_g^G z_{gt} & \leq P_{gt}^G \leq \bar{P}_g^G z_{gt} & \forall g \in \mathcal{G} \quad \text{(1e)} \\ z_{it} & \geq x_{dt} & \forall i \in \mathcal{B}, d \in \mathcal{D}_i \quad \text{(1f)} \\ z_{it} & \geq z_{gt} & \forall i \in \mathcal{B}, g \in \mathcal{G}_i \quad \text{(1g)} \\ z_{it} & \geq z_{ijt} & \forall i \in \mathcal{B}, (i,j) \in \mathcal{L} \quad \text{(1h)} \\ z_{it} & \geq z_{jit} & \forall i \in \mathcal{B}, (j,i) \in \mathcal{L} \quad \text{(1i)} \\ z_{ct} & \geq z_{c \min\{t+1,T\}} & \forall c \in \mathcal{C} \quad \text{(1j)} \\ z_{ct} & \in \{0,1\} & \forall c \in \mathcal{C}. \quad \text{(1k)} \end{split}$$

The objective function considers the expected cost, which consists of the load-shedding cost before the disruption and the total cost after the disruption. Constraints (1a)-(1e) correspond to the DC power flow model and constraints (1f)-(1i) model the component interactions, equivalent to constraint (7)–(9) in [8]. Constraints (1j) describe the temporal logic of components' status: once a component is shut off, it stays off, and the corresponding z variable is 0. The scenario tree of this two-stage SMIP model is shown as Fig. 2, in which each node represents the decisions at a time period, and each branch extending to the right represents a disruption scenario. The black box of the left diagonal branch represents the nominal plan obtained if no disruption occurs. Suppose we have a scenario ω with $\tau^{\omega}=2$. The red box on the right describes the decisions associated with such value function f^{ω} , and the red node implies the disruption time $\tau^{\omega}=2$. The branches in the blue box are the scenarios that are disrupted in period 4 and share the same historical information (the nodes in blue).

We define the expected total cost after the disruption $\sum_{\omega \in \Omega} p^{\omega} f^{\omega}(\cdot, \xi^{\omega})$ as our wildfire risk measure. For each scenario, the second-stage value function f^{ω} takes in the shut-off state variables $\hat{z}_{\cdot \tau^{\omega}-1}$ and the disruption uncertainty ξ^{ω} as its input. It focuses on the operations after τ^{ω} and can be evaluated

by solving the following mixed-integer program:

$$\begin{split} f^{\omega}(\hat{z}_{\tau^{\omega}-1},\xi^{\omega}) \\ &= \min \quad \sum_{t=\tau^{\omega}}^{T} \sum_{d \in \mathcal{D}} w_d (1-x_{dt}^{\omega}) + \sum_{c \in \mathcal{C}} r_c \eta_c^{\omega} \\ \text{s.t.} \quad \forall t \in \{\tau^{\omega}, \dots, T\} : \\ P_{ijt}^{L,\omega} &\leq -b_{ij} \left(\theta_{it}^{\omega} - \theta_{jt}^{\omega} + \bar{\theta}(1-y_{ij}^{\omega})\right) \quad \forall (i,j) \in \mathcal{L} \quad \text{(2a)} \\ P_{ijt}^{L,\omega} &\geq -b_{ij} \left(\theta_{it}^{\omega} - \theta_{jt}^{\omega} + \underline{\theta}(1-y_{ij}^{\omega})\right) \quad \forall (i,j) \in \mathcal{L} \quad \text{(2b)} \\ -W_{ij}y_{ij}^{\omega} &\leq P_{ijt}^{L,\omega} &\leq W_{ij}y_{ij}^{\omega} \qquad \forall (i,j) \in \mathcal{L} \quad \text{(2c)} \\ \sum_{g \in \mathcal{G}_i} P_{gt}^{G,\omega} + \sum_{l \in \mathcal{L}_i} P_{lt}^{L,\omega} &= \sum_{d \in \mathcal{D}_i} D_{dt}x_{dt}^{\omega} \qquad \forall i \in \mathcal{B} \quad \text{(2d)} \\ P_g^{G,\omega}y_g^{\omega} &\leq P_{gt}^{G,\omega} &\leq \bar{P}_g^{G,\omega}y_g^{\omega} \qquad \forall g \in \mathcal{G} \quad \text{(2e)} \\ y_i^{\omega} &\geq x_{dt}^{\omega} \qquad \forall i \in \mathcal{B}, d \in \mathcal{D}_i \quad \text{(2f)} \\ y_i^{\omega} &\geq y_{ij}^{\omega} \qquad \forall i \in \mathcal{B}, (i,j) \in \mathcal{L} \quad \text{(2h)} \\ y_i^{\omega} &\geq y_{ij}^{\omega} \qquad \forall i \in \mathcal{B}, (i,j) \in \mathcal{L} \quad \text{(2h)} \\ y_i^{\omega} &\geq y_{ij}^{\omega} \qquad \forall c \in \mathcal{C} \quad \text{(2j)} \\ y_c^{\omega} &\leq 1 - \eta_c^{\omega} \qquad \forall c \in \mathcal{C} \quad \text{(2l)} \\ \eta_k^{\omega} &\geq v_c^{\omega} \qquad \forall c \in \mathcal{C} \quad \text{(2l)} \\ \eta_k^{\omega} &\geq v_c^{\omega} \qquad \forall c \in \mathcal{C} \quad \text{(2l)} \\ z_c^{\omega} &= \hat{z}_{c\tau^{\omega}-1} \qquad \forall c \in \mathcal{C} \quad \text{(2n)} \\ y_c^{\omega}, \eta_c^{\omega}, z_c^{\omega} &\in \{0,1\} \qquad \forall c \in \mathcal{C}. \quad \text{(2o)} \end{split}$$

The objective function includes the load-shedding cost after the disruption and the wildfire damage cost. The wildfire damage cost for a component $c \in \mathcal{C}$, denoted by r_c , consists of the replacement cost of the electric components and the financial loss to the nearby communities. In model (2), the energization status will stay the same in the remaining time horizon, as we assume that all wildfire damages reveal at period τ^{ω} and no recovery decisions take place afterward. Constraints (2a)–(2e) model an equivalent form of the DC power flow constraints as in model (1). Constraints (2f)–(2i) indicate the functioning state of components, similar to their first-stage counterparts (1f)–(1i). We create a local copy of the first-stage shut-off decisions, z_c^{ω} , via the nonanticipativity constraint (2n), which ensures that the shut-off state of each component at the time of wildfire disruption is identical for all scenarios that share the same history. The binding relationship is illustrated by Fig. 2 and discussed in detail in [29]. With z_c^{ω} indicating whether component c has been shut off, constraint (2j) makes sure that the shut-off components stay down through the second stage. Constraint (2k) states that damaged components no longer function, where we model the exogenous fire damage by constraint (21) and the endogenous fire damage by constraint (2m). Notice that an endogenous fire started at component c requires both a fault occurrence $u_c^{\omega} = 1$ and the component not being shut off $z_c^{\omega}=1$ and spreads to components $k\in I_c^{\omega}$.

III. DECOMPOSITION ALGORITHM BASED ON LAGRANGIAN CUT

The value function f^ω is a non-convex function without an analytical form, as we need to solve a MIP subproblem (2) to evaluate it. A common way to solve model (1) is to replace f^ω with closed-form approximation, such as linear cutting planes. If the state variables are binary, we can generate Lagrangian cuts to equivalently reformulate f^ω as a convex piecewise linear function for each $\omega \in \Omega$ [30]. Such Lagrangian cuts can be applied to model (1) as well because our state variables z are binary. In this section, we first show the derivation of the Lagrangian cut and the convergence properties of the cutting plane method. In addition, we propose an improved Lagrangian cut, square-minimization cut (SMC), and illustrate how it can accelerate the cutting plane algorithm.

At ℓ -th iteration, we solve a Lagrangian dual problem (3) to obtain the cut intercept $v^{\omega,\ell}$ as its optimal value v^* and gradient $\lambda^{\omega,\ell}$ as the optimal solution λ^* . It is worth noting that model (3) is a convex program and we can efficiently solve it using convex programming algorithms, such as the bundle method with stabilization techniques [37]:

$$v^* = \max_{\lambda} R^{\omega}(\hat{z}, \lambda), \tag{3}$$

where the Lagrangian relaxation problem $R^{\omega}(\hat{z}, \lambda)$ is obtained by relaxing the nonanticipativity constraint (2n):

$$R^{\omega}(\hat{z}, \lambda) = \min \sum_{t=\tau^{\omega}}^{T} \sum_{d \in \mathcal{D}} w_d (1 - x_{dt}^{\omega})$$
$$+ \sum_{c \in \mathcal{C}} [r_c \eta_c^{\omega} + \lambda_c (\hat{z}_{c,\tau^{\omega} - 1} - z_c^{\omega})]$$

s.t. Constraints
$$(2a)$$
– $(2m)$, $(2o)$. (4)

Since we can always find a feasible solution to subproblem (2) by setting all variables in model (2) to zero, we do not need to generate feasibility cuts to characterize the domain of f^{ω} and can focus on generating optimality cuts to approximate f^{ω} [28]. For a specific ω , we denote the lower approximation of f^{ω} by V^{ω} , and write the ℓ -th cut as follows:

$$V^{\omega} \ge v^{\omega,\ell} + (\lambda^{\omega,\ell})^{\top} (z_{\tau^{\omega}-1} - \hat{z}_{\tau^{\omega}-1}^{\ell}). \tag{5}$$

With construction of L-1 Lagrangian cuts (5), we can substitute the function f^{ω} by to obtain the lower approximation for model (1) as (M_L) . Since the cuts form a lower approximation of f^{ω} , the optimal value Z_L^* is a lower bound of Z^* .

$$(M_L) \quad Z_L^* = \min \quad \sum_{\omega \in \Omega} p^{\omega} \left[\sum_{t=1}^{\tau^{\omega} - 1} w_d (1 - x_{dt}) + V^{\omega} \right]$$
s.t. Constraints (1a)–(1j)
$$V^{\omega} \ge (\lambda^{\omega, \ell})^{\top} (z_{\tau^{\omega} - 1} - \hat{z}_{\tau^{\omega} - 1}^{\ell})$$

Algorithm 1: Decomposition Algorithm Based on Lagrangian Cuts to Solve Model (1).

```
1 Initialization cut iteration number \ell = 1, lower bound LB = 0,
      upper bound UB = \infty and \epsilon \geq 0;
2 while \frac{UB-LB}{UB} \ge \epsilon do
          /* Forward Steps
          Solve the master problem (M_{\ell}) and obtain the first-stage
           shut-off solution \hat{z}^\ell, optimal value Z_\ell^*, and the
            approximations of value function \hat{V}^{\omega,\ell}
          Update LB = Z_{\ell}^*;
          for \omega \in \Omega do
5
           Solve model (2) with \hat{z}^{\ell} and obtain f^{\omega}(\hat{z}^{\ell}_{\tau\omega}, \xi^{\omega});
6
         Let ar{Z} = Z_\ell^* + \sum_{\omega \in \Omega} p^\omega (f^\omega(\hat{z}_{.\tau\omega}^\ell, \xi^\omega) - \hat{V}^{\omega,\ell}); if ar{Z} < UB then
               Update UB = \bar{Z} and incumbent solution as z^* = \hat{z}^{\ell};
10
         end
          /* Backward Steps
                                                                                           */
         for \omega \in \Omega do
12
               Solve the Lagrangian dual problem (3), and obtain the
13
                 optimal solution \lambda^{\omega,\ell} and the optimal value
                  v^{\omega,\ell} = R^{\omega}(\hat{z}^{\ell}, \lambda^{\omega,\ell});
               And add cut (5) to (M_{\ell});
14
15
16
          Let \ell = \ell + 1;
18 Output the \epsilon-optimal value UB and solution z^*.
```

$$+v^{\omega,\ell}, \quad \forall \omega \in \Omega, \ell = 1, \dots, L-1.$$
 (6)

Once we obtain the optimal solution $(\hat{x},\hat{z},\hat{V},\hat{P})$ to (M_L) , it is a feasible solution to model (1) and we can calculate an upper bound by evaluating $f^\omega(\hat{z}_{.\tau^\omega-1},\xi^\omega)$ for each $\omega\in\Omega$. We present the detailed steps of the decomposition algorithm in Algorithm 1 below, which iteratively updates the bounds. In the end, we terminate Algorithm 1 once the relative gap is within a predefined tolerance threshold $\epsilon\geq0$. We can show that Algorithm 1 converges to the optimal value in finite steps.

Theorem 1 (Convergence): When $\epsilon = 0$, Algorithm 1 terminates in a finite number of iterations and outputs an optimal solution to model (1) after finitely many iterations L.

Proof: According to Theorem 3 in Ref. [30], for a given incumbent first-stage solution \hat{z} and scenario ω , the Lagrangian cut generated at \hat{z} is proven to be tight, meaning that its value at \hat{z} is equal to the value function $f^{\omega}(\hat{z}_{\cdot,\tau^{\omega}-1},\xi^{\omega})$ at this particular point. Since all state variables are binary, there is a finite number of distinct first-stage solutions z, allowing us to fully describe the value function using a finite number of Lagrangian cuts. Consequently, there exists a finite iteration number k_1 , after which no new cuts are generated. For any iteration $k > k_1$, with the resulting first-stage state variable \hat{z}^k and approximate second-stage value function values $\{V^{\omega,k}\}_{\omega\in\Omega}$, two cases may arise: 1) for each scenario ω , $V^{\omega,k}=f^{\omega}(\hat{z}^k_{,\tau^{\omega}-1},\xi^{\omega})$; in this scenario, the resulting upper bound \bar{Z} equals the optimal value of the master problem Z_k^* , leading the algorithm to terminate with a global optimum; 2) there exists a scenario ω such that $V^{\omega} < f^{\omega}(\hat{z}^{k}_{\cdot,\tau^{\omega}-1},\xi^{\omega});$ in this case, a Lagrangian cut is generated to enhance the approximation of the second-stage value

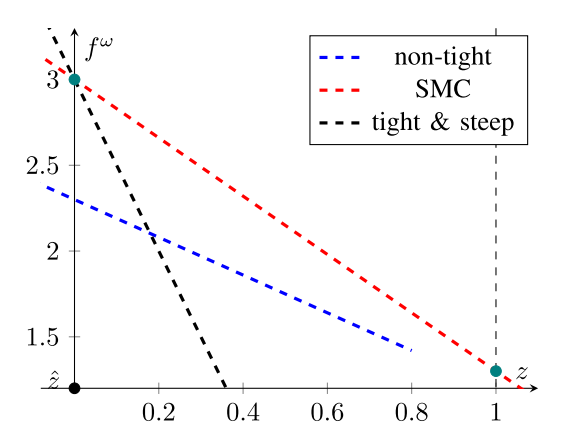


Fig. 3. Illustration of different types of cuts: the black cut and the red cut are tight at $\hat{z} = 0$, but the blue cut is not since its value at \hat{z} is smaller than the function value; the red cut has better performance than the black cut as it also characterizes the function value exactly at another $\hat{z} = 1$.

function. However, this contradicts the result that no new cuts are generated after iteration k_1 . Consequently, the algorithm converges to a global optimum in a finite number of steps. \Box

Although the Lagrangian cut (5) is tight and valid at the incumbent binary solution \hat{z} and results in finite convergence, the cut may be steep and not provide a good lower approximation at other solutions (shown as the black line in Fig. 3). Therefore, We propose a rotated cut, the SMC, which is illustrated by the red line in Fig. 3. Instead of solving model (3) to obtain the cut coefficients λ and v, we solve an alternative model:

$$\min_{\lambda} \quad \lambda^{\top} \lambda \tag{7a}$$
 s.t. $R^{\omega}(\hat{z}, \lambda) \ge (1 - \delta) f^{\omega}(\hat{z}_{\tau^{\omega} - 1}, \xi^{\omega}), \tag{7b}$

s.t.
$$R^{\omega}(\hat{z}, \lambda) > (1 - \delta) f^{\omega}(\hat{z}_{.\tau^{\omega} - 1}, \xi^{\omega}),$$
 (7b)

and we let $\lambda^{\omega,\ell}$ equal to its optimal solution λ^* and $v^{\omega,\ell}$ $R^{\omega}(\hat{z},\lambda^*)$. Fig. 3 shows that the difference between a steep cut and a flat cut lies in the angle they make with the horizontal plane. We prefer a flat cut with a smaller $\lambda^{\top}\lambda$, as λ represents the linear cut's coefficients. While we minimize $\lambda^{\top}\lambda$ and rotate the cut, it is possible that the cut becomes non-tight at the incumbent solution \hat{z} . Therefore, we set up constraint (7b) to force the cut value to be within a δ neighborhood of f^{ω} at \hat{z} , which can be considered an "anchor point." Model (7) is always feasible as the Lagrangian cut coefficients obtained from solving model (3) can serve as a feasible solution. As the function R^{ω} is a concave function of λ given \hat{z} , constraint (7b) characterizes a convex set and we can again use convex programming solution methods to solve model (7).

IV. NUMERICAL RESULTS

In this section, we first describe the numerical experiment setup, with which we evaluate the efficiency of our decomposition method and the solution quality. We then compare our two-stage SMIP model (1) with four benchmark cases: a deterministic model that ignores wildfire disruption, a wait-and-see model with perfect wildfire information, a model based on an aggregate wildfire risk metric, and a robust optimization model that seeks to minimize the total cost of the worst-case scenario.

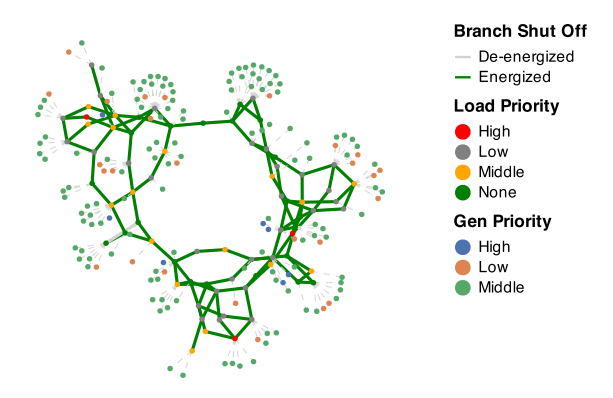


Fig. 4. Illustration of the RTS-GMLC system.

Finally, we examine the robustness of our nominal solution against potential inaccuracy in wildfire disruption probability.

A. Experiment Setup

We use the RTS-GMLC 73-bus case [32] and run experiments on a 24-hour horizon with each time period accounting for an hour (T=24). We assume a constant electricity demand except for the peak hours, 9 am to 12 pm and 3 pm to 7 pm, during which the demand is 1.2 times the non-peak value.

The economic loss caused by fire and sudden power outages depends on the fire intensity and the amount of load in the affected area. To quantify the economic impact of wildfire damage and load loss, we assign each electrical component a numerical rating based on its importance and impact on the area, following a similar approach to the Value Response Index in Texas Wildfire Risk Rating System [38]. We assign each electrical component a scaled cost based on value data from [39], [40], [41], and [42] to create comparable cost values for equipment damage and shed load. We obtain the following cost parameters:

- 1) Load priorities w_d range from 50 to 1000;
- 2) The damage costs r_c of wind turbines, thermal and nuclear power plants are 50, 1000, and 2500, respectively;
- 3) The damage cost r_c of each bus is 50;
- 4) The damage cost r_c of a transmission line is 0.285ℓ , where ℓ is the length of the transmission line.

Fig. 4 color codes the load and generator priority levels based on their load-shedding and damage costs, respectively.

All optimization models were implemented using JuMP [43] in Julia v1.6 [44] and solved by Gurobi v9.5.1 [45] on a computer with a 10-core M1 Pro CPU and 32 GB memory. The network plots are generated using PowerPlot.jl, which depends on PowerModels.jl package [46]. Scenario simulation is constructed by an agent-based model package, Agent.jl [47]. For Algorithm 1 and SMC, we set $\epsilon = 1\%$ and $\delta = 10^{-4}$.

B. Computational Performance and Solution Analysis

We examine how the algorithm performance and solution quality change with sample size. Our two-stage SMIP model, utilizing a set of scenarios Ω , can be considered sample average approximation (SAA) and serve as a lower bound estimator of the optimal value for the true stochastic process of wildfire

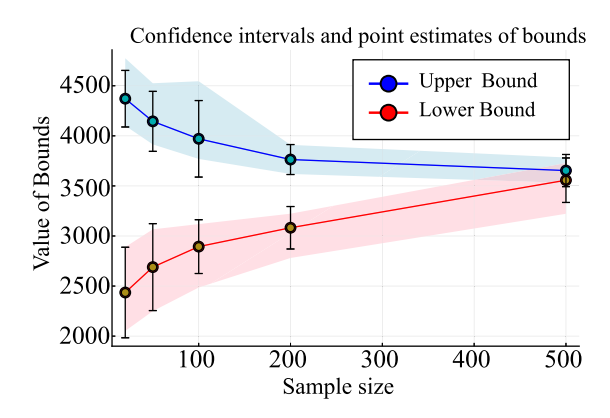


Fig. 5. Confidence intervals (bar) and point estimates (circle) of the lower and upper bounds for solutions with different sample sizes. The shaded area indicates the range of extreme values (maximum and minimum).

TABLE I RUN-TIME (SEC.) OF ALGORITHM 1 UTILIZING SMC AND LC WITH A TOLERANCE OF 1.0%, COMPARED WITH A RUN-TIME OF SOLVING MODEL (1) BY GUROBI WITH MIPGAP = 1%

Sample size	Algorithm SMC (Sec.)	Gurobi Time (Sec.)		
		LC (Sec.)	` /	
20	712	3287	84	
50	1248	8741	376	
100	2604	17911	1510	
200	5323	> 18000	9186	
500	12776	> 18000	> 18000	

progress. As the number of scenarios increases, the approximation precision improves, but the required computational effort also increases [28]. Our objective is to determine a sample size that yields a high-quality solution within an acceptable computational budget. To achieve this, we first obtain twenty first-stage SAA solutions $\hat{X} = \{\hat{x}, \hat{z}, \hat{\theta}, \hat{P}\}$ and optimal values with sample sizes of 20, 50, 100, 200, and 500.

Next, we generate n=5,000 wildfire scenarios $\tilde{\Omega}$ using the procedure outlined in Section II-A for the out-of-sample test. We evaluate the expected total cost of each SAA solution using those 5,000 scenarios as follows:

$$g_n(\hat{X}) = \min \sum_{\omega \in \tilde{\Omega}} \frac{1}{n} \left[\sum_{t=1}^{\tau^{\omega} - 1} \sum_{d \in \mathcal{D}} w_d (1 - \hat{x}_{dt}) + f^{\omega} (\hat{z}_{\cdot \tau^{\omega} - 1}, \xi^{\omega}) \right].$$
(8)

Such cost can serve as an upper-bound estimator for the true wildfire progress. We take the mean of those twenty lower-and upper-bound estimators and calculate their 95% confidence intervals for each sample size, shown in Fig. 5. As the figure illustrates, the gap between the lower- and upper-bound estimators narrows, and both estimators become less variable with increasing sample size. We consider this gap acceptable for a sample size of 500.

As the sample size increases, solving the SMIP model (1) becomes increasingly challenging. Table I shows the effectiveness of Algorithm 1 with SMC. With a sample size of 500, this

algorithm is capable of solving the model within a reasonable time frame (18,000 seconds). In contrast, state-of-the-art solvers like Gurobi are unable to handle such a problem. Table I highlights the necessity of computational improvement through the use of SMC, as the algorithm with the original Lagrangian cuts (LC) fails to reach the optimal solution within the given time constraint.

We simulate scenarios and solve the two-stage SMIP offline in advance of a specific day of operations, which provides a nominal plan. During the day, we execute the nominal plan until a wildfire disruption occurs. Given the wildfire disruption realization, we can solve the second-stage problem to obtain recourse decisions, a process that typically takes less than a second. Therefore, the run-time of Algorithm 1 is sufficient for the practical implementation of our model.

The nominal plan obtained by model (1) balances the trade-off between minimizing load-shedding cost and reducing wildfire risk. For example, transmission line 72 has a high risk of starting an endogenous wildfire, as it ranks 10-th among all transmission lines regarding the number of scenarios where an endogenous wildfire occurs. However, in a 24 time-period horizon, the nominal plan does not de-energize it early because it connects to a bus with multiple generators that supply a large amount of load; see Fig. 6(a). To illustrate this trade-off, we compare the outcomes of de-energizing and keeping line 72 energized. If we intentionally de-energize line 72 early at t = 12, it causes a significant loss of generation and load-shed; see Fig. 6(b). The load-shedding cost outweighs the expected damage cost caused by line 72, so the nominal plan prefers to keep it energized. However, after period 22, the nominal plan de-energizes it (Fig. 6(c)) because the expected damage cost from its fault exceeds the load-shedding cost from less generation. We observe a similar "end-of-horizon" effect when we extend the time horizon length to T=36 and T = 48.

C. Benchmark Comparison

We choose the best optimal solution obtained from twenty batches with a sample size of 500 in Section IV-B as the solution to our two-stage SMIP model (1), denoted as $X^* = \{x^*, z^*, \theta^*, P^*\}$. We then compare this optimal solution, X^* , to the following three benchmark models:

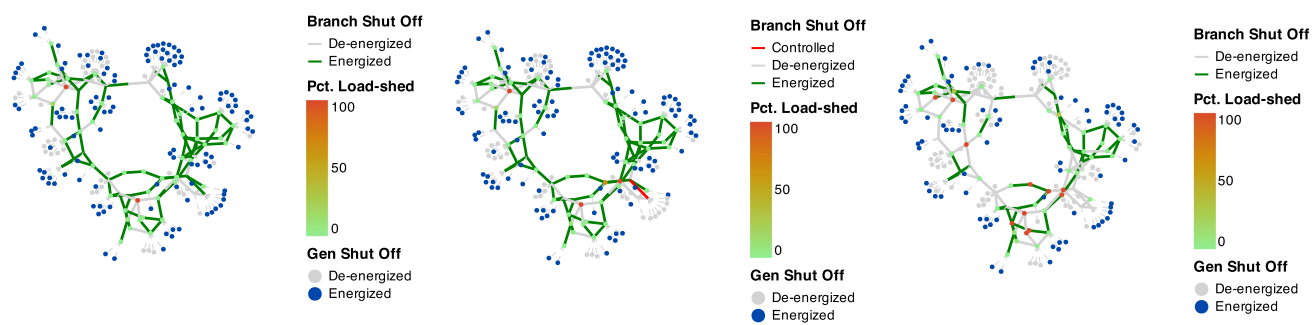
1) A deterministic model where we maximize load satisfaction without considering possible disruption:

$$(M^{det})$$
 min $\sum_{t=1}^{T} \sum_{d \in \mathcal{D}} w_d (1 - x_{dt})$

s.t. Constraints (1a)–(1j).

Since (M^{det}) does not consider the wildfire risk, the optimal solution will return a nominal plan $X^{det} = \{x^{det}, z^{det}, \theta^{det}, P^{det}\}$ with no shut-off.

2) A wait-and-see model where we can make a scenariospecific plan assuming ξ^{ω} is known before we make



- (a) The nominal load plan for the period 12 and its associated load-shedding percentage illustrates how the nominal plan optimizes the load distribution and minimizes the risk exposure under uncertainty.
- (b) The additional load shed in period 12 when transmission line 72 is de-energized intentionally, compared to when the nominal plan keeps it on.
- (c) The nominal load plan for period 22, illustrates how the nominal plan optimizes the load distribution and minimizes the risk exposure under uncertainty.

Fig. 6. Visualization of trade-off in the nominal plan. The red line in the bottom-right corner represents transmission line 72.

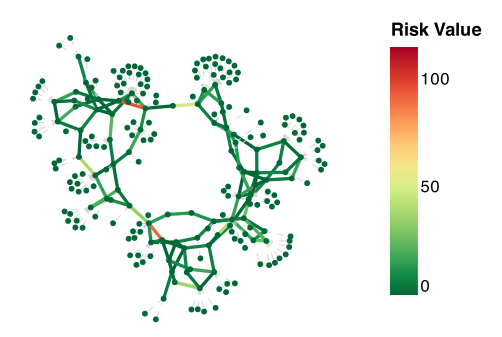


Fig. 7. Illustration of wildfire risk R_{ct} at t = 13.

decisions. For each $\omega \in \Omega$, we solve

$$(M^{ws,\omega}) \quad g^{ws,\omega}$$

$$= \min \quad \sum_{t=1}^{\tau^{\omega}-1} \sum_{d \in \mathcal{D}} w_d (1 - x_{dt}) + f^{\omega}(z_{\tau^{\omega}-1}, \xi^{\omega})$$
s.t. Constraints (1a)–(1j).

and obtain a scenario-specific solution $X^{ws,\omega}=\{x^{ws,\omega},z^{ws,\omega},\theta^{ws,\omega},P^{ws,\omega}\}$. An expected wait-and-see cost can then be computed as $g_n^*=\sum_{\omega\in\Omega}\frac{1}{n}g^{ws,\omega}$.

3) A wildfire-risk-based model proposed by [18] to simultaneously reduce wildfire risk and load-shedding:

$$(M^{rb}) \quad \text{min} \quad \sum_{t=1}^T \left[\frac{\alpha R_{Fire,t}}{R_{Tot}} - (1-\alpha) \frac{\sum_{d \in \mathcal{D}} x_{dt} w_d D_{dt}}{D_{Tot}} \right]$$

s.t. Constraints (1a)–(1j)

$$R_{Fire,t} = \sum_{c \in \mathcal{C}} R_{ct} z_{ct} \quad \forall t \in \mathcal{T},$$

The component-wise risk measure R_{ct} is the mean number of components affected by an endogenous fire started at component c across all scenarios. Fig. 7 illustrates the value of R_{ct} for t=13. The components that face significant wildfire risk are marked in the figure. By controlling the number of energized components, we can

compute the total wildfire risk $R_{Fire,t}$ for the period t. We use the total load $D_{Tot} = \sum_{d \in \mathcal{D}, t \in \mathcal{T}} D_{dt}$ and total wildfire risk $R_{Tot} = \sum_{c \in \mathcal{C}, t \in \mathcal{T}} R_{ct}$ as the normalization factors such that we can combine the wildfire risk and the load-shedding in the objective function. The parameter $\alpha \in [0,1]$ adjusts the trade-off between serving loads and reducing wildfire risk. Solving model (M^{rb}) returns a nominal plan $X^{rb,\alpha} = \{x^{rb,\alpha}, z^{rb,\alpha}, \theta^{rb,\alpha}, P^{rb,\alpha}\}$.

4) A scenario-based robust optimization model, in which we minimize the total cost of the worst-case scenario:

$$(M^{ro}) \min \max_{\omega \in \Omega} \sum_{t=1}^{\tau^{\omega}-1} \sum_{d \in \mathcal{D}} w_d (1-x_{dt}) + f^{\omega}(z_{\tau^{\omega}-1}, \xi^{\omega})$$

Solving model (M^{ro}) returns a nominal plan $X^{ro} = \{x^{ro}, z^{ro}, \theta^{ro}, P^{ro}\}.$

Each model is solved, then evaluated with the same n = 5,000 out-of-sample scenarios $\tilde{\Omega}$ used to evaluate the two-stage SMIP model (1). For the deterministic model and the wait-and-see model, we obtain two following ratios to show their relative difference compared to model (1):

$$\frac{g_n(X^{det})-g_n(X^*)}{g_n(X^*)}=0.639 \text{ and } \frac{g_n(X^*)-g_n^*}{g_n(X^*)}=0.416.$$

The first ratio emphasizes that the two-stage SMIP can significantly improve the operations compared to the deterministic approach agnostic to potential wildfires. The second ratio quantifies the value of perfect information. We can save 41.6% of the cost if we can forecast the wildfire perfectly before we make the shut-off decisions. This large ratio reflects the high variance in wildfire scenarios and the difficulty for a single nominal shut-off plan to perform optimally in all scenarios. While it is not entirely possible to obtain the perfect information, it is helpful if we can obtain auxiliary data, conditioned on which we can identify a better representation of the scenarios. For example, we may exclude the scenarios with wildfires occurring in areas with forecast precipitation.

Fig. 8 illustrates such effect by selecting a subset of twenty scenarios: we can observe that the cost of the SMIP solution is

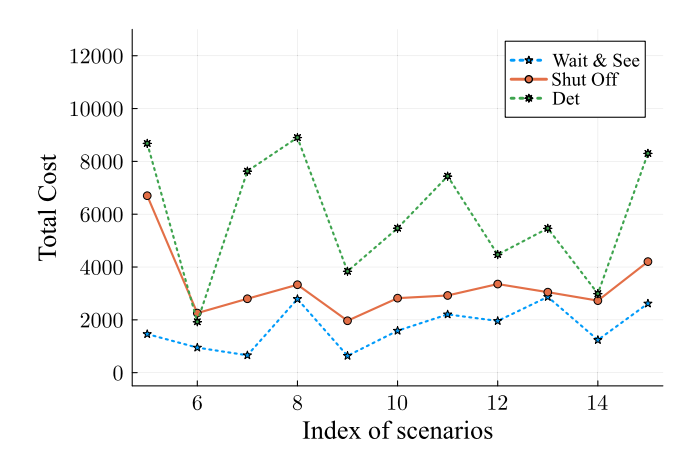


Fig. 8. Scenario-specific costs for model (1), the deterministic model (M^{det}) , and the wait-and-see model $(M^{ws,\omega})$. For each scenario, the green star and orange circle represent the costs incurred by the nominal plans generated by (M^{det}) and model (1). The blue star marks the wait-and-see cost.

TABLE II LOAD-SHEDDING COSTS AND DAMAGE COSTS OF NOMINAL PLANS $X^{rb,\alpha}$ Under Non-Disruptive and Disruptive Scenarios

	Non-Disr.	Disrut	otive	Total Cost		
α	Load shed	Load shed	Damage	$g_n(\cdot)$	RRI	
$0.0/X^{det}$	0.0	3247.0	2814.0	5936.2	63.9%	
0.1	148.6	3843.5	1767.5	5495.4	51.7%	
0.2	162.9	3850.7	1739.8	5480.8	51.4%	
0.3	221.4	3891.0	1713.9	5489.4	51.6%	
0.4	171.6	3786.3	1783.4	5454.9	50.6%	
0.5	251.1	3712.8	1773.9	5373.7	48.4%	
0.6	106.7	3686.8	1817.0	5390.5	48.9%	
0.7	469.3	3721.4	1754.1	5425.9	50.0%	
0.8	883.6	3949.0	1700.1	5532.7	52.8%	
0.9	1505.8	4285.3	1341.1	5510.5	52.2%	
X^*	1678.2	2355.2	1333.6	3612.7	0.0%	

significantly lower than the cost of the deterministic solution in all but one of the selected scenarios and can approach the best possible cost in two scenarios. If the auxiliary data happen to show those two scenarios are likely to happen, our SMIP solution will perform well. On the contrary, if the auxiliary data tell the other way, we may want to re-solve the two-stage SMIP model 1 with a refined set of scenarios.

For the wildfire-risk-based model (M^{rb}) , we use the set of scenarios Ω^* , with which we obtain X^* , to calculate the wildfire risk value $R_{Fire,t}$ for all $t \in \mathcal{T}$. We obtain a solution $X^{rb,\alpha}$ for $\alpha \in \{0.0,0.1,\ldots,0.9\}$. We list the out-of-sample mean load-shedding cost and wildfire damage cost under non-disruptive scenarios (no wildfire ignitions) and disruptive scenarios in Table II, evaluated with Ω .

If the wildfire risk is ignored ($\alpha=0.0$), it is equivalent to the deterministic solution X^{det} , which leads to a large out-of-sample cost $g_n(X^{det})$. By increasing α , we can first reduce the total cost via the preventive shut-offs of potentially risky components, resulting in less damage cost. However, as α increases further, the nominal plan becomes too conservative, and many components are de-energized such that the increasing load-shedding cost outweighs the reduced damage costs. This illustrates a major

TABLE III LOAD-SHEDDING COSTS AND DAMAGE COSTS OF NOMINAL PLANS X^{ro} Under Non-Disruptive and Disruptive Scenarios

Non-Dist	: Disru	ptive	ive Cost		
Load she	d Load shed	Damage	$g_n(\cdot)$	Worst-case	
$X^{ro} \mid 30130.2$	18067.3	2506.3	20770.5	56848.3	
$X^* \mid 1678.2$	2355.2	1333.6	3612.7	28871.1	

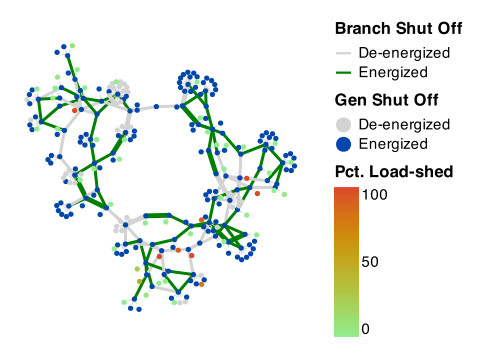


Fig. 9. Illustration of the power system under the nominal plan X^{ro} at time t=16.

challenge in the wildfire-risk-based model (M^{rb}) as there is little guidance to select a proper α .

We then compare our SMIP model (1) with the wildfire-riskbased model (M^{rb}) , via the ratio of relative improvements (RRI) $(g_n(X^{rb,\alpha})-g_n(X^*))/g_n(X^*)$ in Table II. The results show that the nominal plan obtained by solving model (1) performs significantly better, and the RRI values for $X^{rb,\alpha}$ exceed 45% for all α selected. This indicates that, without considering wildfire scenarios and potential adaptive recourse actions, static nonrobust planning is far from optimum, regardless of the level of conservatism. The reason is that (M^{rb}) only considers minimizing the total wildfire risk and satisfying the power demand, which leads to the nominal plans that de-energize any component with $R_{ct} > 0$ for some $t \in \mathcal{T}$ as early as possible, only if this action does not affect the future supply of electricity. However, this property may compromise the resilience of the power grid by de-energizing an excessive number of components. If a disruption occurs, there might be very high load-shedding costs.

We use a scenario-appending algorithm similar to that in Ref. [48]. The algorithm starts with solving a relaxed model considering only a prespecified subset of scenarios $\hat{\Omega} \subset \Omega^*$ and obtains a solution \hat{X} . An oracle is run to find the worst-case scenario $\hat{\omega} \in \Omega^*$ given \hat{X} . We append such a scenario to the set $\hat{\Omega}$ and repeat the above process until the obtained $\hat{\omega}$ is already in $\hat{\Omega}$. The experiment demonstrates that the subset $\hat{\Omega}$ includes 23 scenarios, much smaller than $|\Omega^*| = 500$, allowing us to run the algorithm in 109 seconds. Although the robust optimization algorithm runs faster, the robust solution X^{ro} presents worse out-of-sample test results using scenario set $\tilde{\Omega}$ in Table III, compared with those of the SMIP solution X^* . The robust nominal plan X^{ro} de-energizes more components early in the time horizon to mitigate endogenous wildfire risks, which is illustrated in Fig. 9. Consequently, this conservative

TABLE IV LOAD-SHEDDING COSTS AND DAMAGE COSTS OF NOMINAL PLANS $X^{\Delta p}$ Under Non-Disruptive and Disruptive Scenarios

	Non-Disr.	Disru	otive	Total Cost		
Δp	Load shed	Load shed	Damage	$g_n(\cdot)$	RRI	
-0.05	1805.1	2553.0	1242.7	3782.8	4.5%	
-0.015	1741.5	2513.7	1353.6	3787.3	4.6%	
$0.0/X^*$	1678.2	2355.2	1333.6	3612.7	0.0%	
0.015	1660.0	2343.9	1341.7	3609.7	-0.1%	
0.05	1504.9	2360.2	1325.4	3609.6	-0.1%	
0.1	1250.7	2344.8	1317.1	3586.5	-0.7%	
0.2	828.4	2196.5	1578.8	3697.5	2.3%	
0.3	207.3	2181.1	1752.3	3882.5	7.3%	
0.5	185.1	2343.5	1845.6	4109.1	13.5%	
0.7	109.7	2410.8	1851.0	4153.3	15.0%	
0.9	99.0	2476.8	1878.1	4276.7	18.4%	

strategy results in a substantial amount of load-shedding in both nominal and disruptive scenarios, leading to a total cost of up to four times that of X^* . The worst-case in-sample cost among scenarios in Ω^* for X^{ro} is 32,374 compared to 34,016 for X^* , which is reasonable as X^{ro} optimizes the worst-case scenario. However, the out-of-sample worst-case costs, as demonstrated in the last column of Table III, indicate that X^{ro} is sensitive to the scenario selection and performs poorly when facing new samples. In contrast, our stochastic programming solution X^* shows robustness as the out-of-sample worst-case cost is even smaller than the in-sample one. Moreover, the performance of X^{ro} significantly lags behind that of X^* across other scenarios. Although the robust model requires less time to generate a feasible nominal plan, the numerical results show that the robust nominal plan is conservative because it relies on limited scenario information and prioritizes minimizing worst-case costs.

D. Sensitivity Analysis of Disruption Probability

We simulate the set of wildfire scenarios with a probabilistic model described in Section II-A, which then serves as the uncertainty model in the SMIP. It is necessary to examine the robustness of the optimal solution to the SMIP against the potential inaccuracy in such an uncertainty model. Therefore, we perform a sensitivity analysis in this section to check the out-of-sample performance of SMIP solutions obtained with different uncertainty assumptions.

In Section II, we construct a scenario set Ω^* in the SMIP model (1), each scenario with an equal probability of occurrence, $1/|\Omega^*|$. Such a scenario set can be partitioned as $\Omega^* = \Omega_D^* \cup \Omega_N^*$, where $\Omega_D^* \left(\Omega_N^* \right)$ represents the set of scenarios with(out) a disruption. When there is no disruption, the nominal plan is carried out over the entire time horizon. Therefore, the partition is equivalent to $\Omega^* = \Omega_D^* \cup \{\omega_0\}$ with probabilities $p^{\omega_0} = |\Omega_N^*|/|\Omega^*|$ and $p^\omega = (1-p^{\omega_0})/|\Omega_D^*|$ for $\omega \in \Omega_D^*$, where ω_0 is a scenario without disruption.

For the sensitivity analysis, we add a perturbation Δp to p^{ω_0} and adjust p^{ω} for $\omega \in \Omega_D^*$ accordingly. We solve the SMIP for each Δp and test its solution's out-of-sample performance over

the scenario set $\tilde{\Omega}$, displayed in Table IV. The out-of-sample no-disruption probability $|\tilde{\Omega}_N|/|\tilde{\Omega}|$ is approximately 0.05, similar to that of Ω^* .

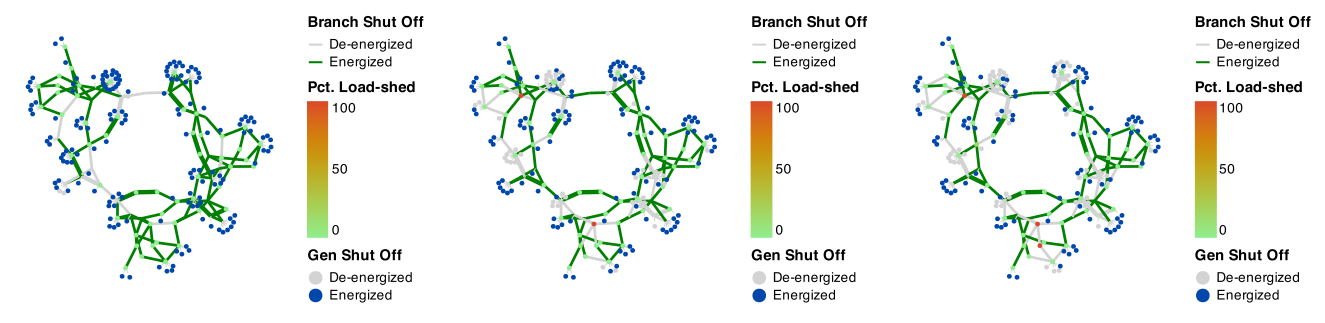
We observe from Table IV that the optimal SMIP solution can yield a decent out-of-sample performance even when the input perturbation is quadruple the original no-disruption probability ($\Delta p=0.2$). This indicates that the SMIP optimal solution is robust against input inaccuracy. When Δp keeps increasing, the SMIP values a nominal plan that shuts off fewer components and thus minimizes the load-shedding cost under scenarios without wildfire disruption. It leads to higher out-of-sample load-shedding and damage costs simultaneously as insufficient shut-offs are executed to prevent endogenous wildfires. The sensitivity analysis results show that the SMIP optimal solution is reliable as long as the input uncertainty model is not too liberal when estimating the wildfire risk.

E. Interaction Between Endogenous and Exogenous Wildfires

In this section, we investigate how endogenous and exogenous wildfires interact and affect the shut-off plans. Intuitively speaking, considering endogenous wildfires tends to encourage more shut-offs to prevent faults ignited by power system components, while the presence of exogenous wildfires introduces additional load-shedding costs which can be mitigated by keeping more components energized. To quantify this interaction, we compare three nominal plans: 1) X^{exo} obtained by solving model (1) with 500 scenarios that only contain exogenous wildfires; 2) X^{end} obtained by solving model (1) with 500 scenarios that only contain endogenous wildfires; and 3) X^* obtained in Section IV-C with 500 scenarios that contain a mixture of exogenous and endogenous wildfires. Fig. 10 illustrates the power system status, highlighting the de-energized components and load-shed in period t = 16. The nominal plan X^{exo} , shown in the left plot, exhibits the fewest number of de-energized components. In contrast, the right plot shows the nominal plan X^{end} leads to the highest number of shut-offs. The nominal plan X^* , considering both exogenous and endogenous wildfires, represents a trade-off between the two. We perform three additional out-of-sample tests to evaluate those nominal plans with 5,000 scenarios of: 1) exogenous wildfires only; 2) endogenous wildfires only; and 3) a mixture of endogenous and exogenous wildfires, as shown in Fig. 10. The nominal plan X^{exo} exhibits inferior performance in both load-shedding and damage costs when endogenous wildfires are possible. The nominal plan X^{end} becomes conservative and shuts off too many components, resulting in consistently high load-shedding costs. While the nominal plan X^* achieves a balance in between. Our finding confirms the intuition of how exogenous and endogenous wildfires interact and highlights the importance of modeling both types of wildfires in power system operations.

V. CONCLUSION & FUTURE WORK

This work contributes to the literature on stochastic optimization for power system operation under wildfire risk. We propose a novel two-stage stochastic program that captures the



(a) 15 transmission lines are de-energized in X^{exo} in period 16. (b) 26 transmission lines are de-energized in X^{exo} in period 16. (c) 31 transmission lines are de-energized in X^{end} in period 16.

Fig. 10. Visualization of interaction between endogenous and exogenous wildfire risk. (a) 15 transmission lines are de-energized in X^{exo} in period 16. (b) 26 transmission lines are de-energized in X^{end} in period 16.

 ${\it TABLE~V}$ Performance of the Nominal Plans Generated From Different Scenarios Under Different Test Sets

Exogenous Wildfire Scenario Set Mixture Wildfire Scenario Set Endogenous Wildfire Scenario Set									Set			
	Non-Disr. Disruptive		Total	Non-Disr.	Disruptive		Total	Non-Disr.	Disruptive		Total	
Type	Load shed	Load shed	Damage	$g_n(\cdot)$	Load shed	Load shed	Damage	$g_n(\cdot)$	Load shed	Load shed	Damage	$g_n(\cdot)$
X^{exo}	0.0	707.1	636.5	1289.8	0.0	3231.8	2961.0	5960.2	0.0	3380.4	2979.8	6106.0
X^*	1678.1	1892.8	636.5	2495.2	1678.2	2355.2	1333.6	3612.7	1678.2	3107.1	1814.0	4792.8
X^{end}	1998.5	2249.9	636.5	2850.9	1998.5	2748.6	1240.3	3909.1	1998.5	3147.0	1514.0	4554.4

uncertainty of wildfire disruptions and temporal dynamics. We also develop an efficient decomposition algorithm that exploits the binary structure of state variables and generates valid cuts for solving large-scale instances. Our numerical experiments demonstrate the effectiveness and robustness of our approach in terms of solution quality and computational speed. They illustrate the benefits of the stochastic programming model by comparing it with deterministic counterparts and the scenario-based robust optimization model.

For future work, we plan to extend our research in several directions. One direction is to investigate a theory-driven approach for generating effective and efficient cuts in our decomposition algorithm. Another direction is to expand the current modeling setting: 1) to relax the assumption of at most one disruption and extend our model to a multistage problem; 2) to include the unit commitment decisions, which would require an algorithmic development to handle the continuous state variables to model the ramping constraints; 3) to formulate a realistic multi-period uncertainty set/ambiguity set based on high-fidelity wildfire simulators and model the wildfire disruption in robust/distributionally robust optimization. A third direction is to address the challenge of ensuring feasibility with AC power flow when using a linear approximation of power flow in our model. Finally, we aim to develop a rolling horizon framework that can handle the wildfire forecast updates and dynamically re-optimize the de-energization schedule.

REFERENCES

 J. W. Muhs, M. Parvania, and M. Shahidehpour, "Wildfire risk mitigation: A paradigm shift in power systems planning and operation," *IEEE Open Access J. Power Energy*, vol. 7, pp. 366–375, 2020.

- [2] T. P. Holmes, R. J. Huggett Jr., and A. L. Westerling, "Statistical analysis of large wildfires," *Econ. Forest Disturbances*, vol. 79, pp. 59–77, 2008.
- [3] D. A. Z. Vazquez, F. Qiu, N. Fan, and K. Sharp, "Wildfire mitigation plans in power systems: A literature review," *IEEE Trans. Power Syst.*, vol. 37, no. 5, pp. 3540–3551, Sep. 2022.
- [4] "2019 Wildfire risk report," CoreLogic, Irvine, CA, USA, Tech. Rep., 2019. [Online]. Available: https://www.corelogic.com/wp-content/uploads/sites/4/downloadable-docs/wildfire-report_0919-01-screen.pdf
- [5] M. Choobineh, B. Ansari, and S. Mohagheghi, "Vulnerability assessment of the power grid against progressing wildfires," *Fire Saf. J.*, vol. 73, pp. 20–28, 2015.
- [6] S. Jazebi, F. D. León, and A. Nelson, "Review of wildfire management techniques—Part I: Causes, prevention, detection, suppression, and data analytics," *IEEE Trans. Power Del.*, vol. 35, no. 1, pp. 430–439, Feb. 2020.
- [7] "Utility public safety power shutoff plans (de-energization)," California Public Utilities Commission (CPUC), 2022. [Online]. Available: https://www.cpuc.ca.gov/psps/
- [8] N. Rhodes, L. Ntaimo, and L. Roald, "Balancing wildfire risk and power outages through optimized power shut-offs," *IEEE Trans. Power Syst.*, vol. 36, no. 4, pp. 3118–3128, Jul. 2021.
- [9] S. Taylor and L. A. Roald, "A framework for risk assessment and optimal line upgrade selection to mitigate wildfire risk," *Electric Power Syst. Res.*, vol. 213, 2022, Art. no. 108592.
- [10] M. Davoudi, B. Efaw, M. Avendaño-Mora, J. L. Lauletta, and G. B. Huffman, "Reclosing of distribution systems for wildfire prevention," *IEEE Trans. Power Del.*, vol. 36, no. 4, pp. 2298–2307, Aug. 2021.
- [11] T. Zhou, B. Li, C. Wu, Y. Tan, L. Mao, and W. Wu, "Studies on Big Data mining techniques in wildfire prevention for power system," in *Proc. IEEE 3rd Conf. Energy Internet Energy Syst. Integration*, 2019, pp. 866–871.
- [12] R. Bayani, M. Waseem, S. D. Manshadi, and H. Davani, "Quantifying the risk of wildfire ignition by power lines under extreme weather conditions," *IEEE Syst. J.*, vol. 17, no. 1, pp. 1024–1034, Mar. 2023.
- [13] W. Hong, B. Wang, M. Yao, D. Callaway, L. Dale, and C. Huang, "Data-driven power system optimal decision making strategy under wildfire events," Lawrence Livermore National Lab, Livermore, CA, USA, Tech. Rep. LLNL-CONF-831390, 2022.
- [14] C. Huang et al., "A review of public safety power shutoffs (PSPS) for wildfire mitigation: Policies, practices, models and data sources," *IEEE Trans. Energy Markets, Policy Regulation*, vol. 1, no. 3, pp. 187–197, Sep. 2023.
- [15] A. Lesage-Landry, F. Pellerin, J. A. Taylor, and D. S. Callaway, "Optimally scheduling public safety power shutoffs," *Stochastic Syst.*, 2023.

- [16] R. Bayani and S. D. Manshadi, "Resilient expansion planning of electricity grid under prolonged wildfire risk," IEEE Trans. Smart Grid, vol. 14, no. 5, pp. 3719-3731, Sep. 2023.
- [17] Y. Zhou, K. Sundar, D. Deka, and H. Zhu, "Optimal power system topology control under uncertain wildfire risk," 2023, arXiv:2303.07558.
- [18] N. Rhodes and L. Roald, "Co-optimization of power line de-energization and restoration under high wildfire ignition risk," 2022, arXiv:2204.02507.
- [19] A. Kody, A. West, and D. K. Molzahn, "Sharing the load: Considering fairness in de-energization scheduling to mitigate wildfire ignition risk using rolling optimization," in Proc. IEEE 61st Conf. Decis. Control, 2022, pp. 5705-5712.
- [20] G. Y. Ke, "Managing reliable emergency logistics for hazardous materials: A two-stage robust optimization approach," Comput. Operations Res., vol. 138, 2022, Art. no. 105557.
- [21] S. Jazebi, F. D. León, and A. Nelson, "Review of wildfire management techniques-Part II: Urgent call for investment in research and development of preventative solutions," IEEE Trans. Power Del., vol. 35, no. 1, pp. 440-450, Feb. 2020.
- [22] S. Li and T. Banerjee, "Spatial and temporal pattern of wildfires in California from 2000 to 2019," Sci. Rep., vol. 11, no. 1, 2021, Art. no. 8779.
- [23] M. Nagpal, R. P. Barone, T. G. Martinich, Z. Jiao, S.-H. Manuel, and S. Merriman, "Wildfire trips de-energized line shunt reactor," IEEE Trans. Power Del., vol. 34, no. 2, pp. 760-768, Apr. 2019.
- [24] H. N. V. Pico and B. B. Johnson, "Transient stability assessment of multimachine multi-converter power systems," IEEE Trans. Power Syst., vol. 34, no. 5, pp. 3504-3514, Sep. 2019.
- [25] J. W. Mitchell, "Power line failures and catastrophic wildfires under extreme weather conditions," Eng. Failure Anal., vol. 35, pp. 726-735, 2013.
- [26] J. H. Scott, M. P. Thompson, and D. E. Calkin, "A wildfire risk assessment framework for land and resource management," U.S. Department of Agriculture, Forest Service, Rocky Mountain Research Station, Fort Collins, CO, USA, Tech. Rep. RMRS-GTR-315, 2013.
- [27] S. Dian et al., "Integrating wildfires propagation prediction into early warning of electrical transmission line outages," IEEE Access, vol. 7, pp. 27586-27603, 2019.
- [28] J. R. Birge and F. Louveaux, Introduction to Stochastic Programming. New York, NY, USA: Springer-Verlag, 1997.
- H. Yang and H. Nagarajan, "Optimal power flow in distribution networks under N-1 disruptions: A multistage stochastic programming approach," INFORMS J. Comput., vol. 34, no. 2, pp. 690-709, 2022
- [30] J. Zou, S. Ahmed, and X. A. Sun, "Stochastic dual dynamic integer programming," Math. Program., vol. 175, no. 1/2, pp. 461–502, 2019.
- [31] J. Freire and C. Dacamara, "Using cellular automata to simulate wildfire propagation and to assist in fire prevention and fighting," Natural Hazards Earth Syst. Sci. Discuss., vol. 19, no. 1, pp. 169–179, 2019.
- [32] C. Barrows et al., "The IEEE reliability test system: A proposed 2019
- update," *IEEE Trans. Power Syst.*, vol. 35, no. 1, pp. 119–127, Jan. 2020. [33] MapTools, "Why use UTM coordinates," 2023. [Online]. Available: https: //www.maptools.com/tutorials/utm/why_use_utm
- [34] "Wildland fire potential index (WFPI)." [Online]. Available: https://www. usgs.gov/fire-danger-forecast/wildland-fire-potential-index-wfpi
- [35] A. Alexandridis, D. Vakalis, C. Siettos, and G. Bafas, "A cellular automata model for forest fire spread prediction: The case of the wildfire that swept through spetses island in 1990," Appl. Math. Comput., vol. 204, no. 1, pp. 191-201, 2008.
- [36] S. Yang et al., "Failure probability estimation of overhead transmission lines considering the spatial and temporal variation in severe weather," J. Modern Power Syst. Clean Energy, vol. 7, no. 1, pp. 131–138, 2019.
- [37] C. Lemaréchal, A. Nemirovskii, and Y. Nesterov, "New variants of bundle methods," Math. Program., vol. 69, no. 1, pp. 111-147, 1995.
- "Texas A&M forest service: Texas wildfire risk assessment portal." [Online]. Available: https://texaswildfirerisk.com/
- [39] World Nuclear Association, "Economics of nuclear power," 2022. [Online]. Available: https://world-nuclear.org/information-library/economicaspects/economics-of-nuclear-power.aspx
- [40] D. Blewett, "Wind turbine cost: How much? Are they worth it in 2022?," 2022. [Online]. Available: https://weatherguardwind.com/howmuch-does-wind-turbine-cost-worth-it/
- [41] World Nuclear Association, "Financing nuclear energy," 2020. [Online]. Available: https://world-nuclear.org/information-library/economicaspects/financing-nuclear-energy.aspx

- [42] "2021 transmission cost report," Australian Energy Market Operator, Australia, Tech. Rep., 2021. [Online]. Available: https: //aemo.com.au/-/media/files/major-publications/isp/2021/transmissioncost-report.pdf?la=en
- [43] I. Dunning, J. Huchette, and M. Lubin, "JuMP: A modeling language for mathematical optimization," SIAM Rev., vol. 59, no. 2, pp. 295-320,
- [44] S. K. J. Bezanson, A. Edelman, and V. Shah, "Julia: A fresh approach to numerical computing," SIAM Rev., vol. 59, no. 1, pp. 65-98, 2014.
- [45] Gurobi Optimization, Inc., "Gurobi optimizer reference manual," 2014. [Online]. Available: https://www.gurobi.com
- C. Coffrin, R. Bent, K. Sundar, Y. Ng, and M. Lubin, "Powermodels.jl: An open-source framework for exploring power flow formulations," in Proc. Power Syst. Comput. Conf., 2018, pp. 1-8.
- [47] G. Datseris, A. R. Vahdati, and T. C. DuBois, "Agents.jl: A performant and feature-full agent-based modeling software of minimal code complexity," Simulation, 2022, doi: 10.1177/00375497211068820.
- [48] H. Yang, D. P. Morton, C. Bandi, and K. Dvijotham, "Robust optimization for electricity generation," INFORMS J. Comput., vol. 33, no. 1, pp. 336-351, 2021.



Hanbin Yang received the B.Sc. degree from the Southern University of Science and Technology, Shenzhen, China, in 2020. He is currently working toward the Ph.D. degree with the School of Data Science, Chinese University of Hong Kong, Shenzhen. His research interests include optimization under uncertainty, integer programming, and their applications in power systems.



Noah Rhodes (Graduate Student Member, IEEE) received the B.Sc. degree in electrical and computer engineering in 2019 from the University of Wisconsin-Madison, Madison, WI, USA, where he is currently working toward the Ph.D. degree with the Department of Electrical and Computer Engineering. His research interests include modeling of large-scale disruptions to power systems and optimization of recovery operations, with a focus on the risk of wildfire ignitions by the power system. He was the recipient of multiple best paper awards, the Wisconsin Distin-

guished Graduate Fellowship and the IEEE Power Engineering Society Student Fellowship.



Haoxiang Yang received the Ph.D. degree in industrial engineering and management sciences from Northwestern University, Evanston, IL, US, in 2019. He is currently an Assistant Professor with the School of Data Science, Chinese University of Hong Kong, Shenzhen, China. He was a Postdoctoral Research Associate with the Center of Non-Linear Studies, Los Alamos National Laboratory, from 2019 to 2021. His current research interests include optimization under uncertainty, large-scale optimization and decomposition methods, mixed integer programming, and non-

linear optimization, with applications focusing on energy systems, disaster relief and humanitarian aid, public health, air transportation, supply chain, and sports analytics.



Line Roald (Member, IEEE) received the Ph.D. degree in electrical engineering from ETH Zurich, Zurich, Switzerland, in 2016. She is currently an Associate Professor and Grainger Institute Fellow in the Department of Electrical and Computer Engineering, University of Wisconsin-Madison (UW Madison), Madison, WI, USA. Prior to joining UW Madison, she was a Postdoctoral Research Fellow with the Center of Non-Linear Studies, Los Alamos National Laboratory. Her research interests center around modeling and optimization of energy systems, with a

particular focus on managing uncertainty and risk from extreme weather and renewable energy variability. She was the recipient of an NSF CAREER Award, several best paper awards and the UW Madison ECE Outstanding Graduate Mentor Award.



Lewis Ntaimo received the B.S. degree in mining engineering the M.S. degree in mining and geological engineering and Ph.D. degree in systems and industrial engineering with a minor in electrical and computer engineering, from the University of Arizona, Tucson, AZ, USA, in 1998, 2000, and 2004, respectively. He is currently a Professor and the Department Head, and the Sugar and Mike Barnes Department Head Chair of the Department of Industrial and Systems Engineering, Texas A&M University, College Station, TX, USA. He has been with Texas

A&M since 2004. His research interests include mathematical models and algorithms for decision-making problems involving data uncertainties and risk in the general area of stochastic optimization, systems and process modeling and optimization, and computer simulation. His current applications of interest include vaccination policies for epidemics, wildfire management, healthcare management, college counseling and psychological service management, and power systems operations and maintenance.